Scientia Marina 72(4)
December 2008, 779-799, Barcelona (Spain)
ISSN: 0214-8358
doi: 10.3989/scimar.2008.72n4779

XBT profilers for operational purposes: application and validation in real exercises

FRANCISCO MACHÍN [1], MIKHAIL EMELIANOV [1], PABLO RODRÍGUEZ [2], EMILIO GARCÍA-LADONA [1], JAVIER MENÉNDEZ [3] and JORDI SALAT [1]

[1] Institut de Ciències del Mar, Centre Mediterrani d'Investigacions Marines i Ambientals (CSIC), Barcelona, Spain.
E-mail: fmachin@icm.csic.es
[2] Unitat de Tecnologia Marina, Centre Mediterrani d'Investigacions Marines i Ambientals (CSIC), Barcelona, Spain.
[3] Sociedad de Salvamento y Seguridad Marítima (SASEMAR), Centro Jovellanos, Gijón, Spain.

SUMMARY: A methodology for recovering salinity from expendable bathythermograph (XBT) data is presented. The procedure exploits climatological relationships between temperature, salinity and depth to build regional characteristic curves by fitting a polynomial function that minimises both the variance of residuals and unknowns. Hence, salinity is computed and recovered as a function of temperature and depth. Empirical formula are provided to recover the salinity field from temperature-depth measurements for the Cantabrian Sea and Galician Area. The method is validated and applied in the context of two marine rescue exercises carried out in the Bay of Biscay close to the north coast of Spain and in the Finisterre region, where a series of XBT and conductivity-temperature-depth (CTD) profiles were acquired during fast samplings. The results agree reasonably well with independent data in terms of the spatial structure, with the largest errors in the upper 100 m of the ocean and at intermediate levels. The first diagnoses of the surface geostrophic velocity fields obtained through the salinity reconstruction are coherent and may help in rescue and safety operations during marine emergencies. Hence, we recommend that a technical unit should consider this kind of expandable sampling strategy with both XBT and XCTD data during marine emergencies, since it provides useful and comprehensive information rapidly with minimal interference by means of formal operations on board search and rescue ships.

Keywords: XBT probes, operational oceanography, inverse method.

RESUMEN: Perfiladores XBT para fines operacionales: aplicación y validación en dos casos reales. – Presentamos una metodología para el cálculo de la salinidad a partir de datos de XBT. El procedimiento hace uso de la relación climatológica S-T-d para construir curvas características de la región ajustando una función polinomial que minimiza tanto la varianza del residuo como de las incógnitas. De esta manera, la salinidad es calculada en función de la temperatura y la profundidad. Estas expresiones empíricas se han empleado para estimar el campo de salinidad a partir de medidas de temperatura y profundidad realizadas en el Mar Cantábrico y en el área de Galicia. El método se ha validado y aplicado en el contexto de dos ejercicios de salvamento marítimo, llevados a cabo en el Golfo de Vizcaya y en la región de Finisterre, donde se lanzaron XBT's en muestreos rápidos y se obtuvieron perfiles de CTD. Los resultados muestran una coherencia razonable al compararlos con datos independientes en términos de la estructura espacial, con errores más importantes en los 100 m superiores de la columna de agua y en capas intermedias. Los primeros diagnósticos de la velocidad geostrófia en superficie son igualmente coherentes y pueden ser de gran ayuda en operaciones de salvamento y rescate durante emergencias en el mar. Por tanto, recomendamos a la Unidad Técnica que en situaciones de emergencia considere la posibilidad de realizar campañas con sondas desechables (XBT's y XCTD's), en tanto que este proceso es rápido, no interfiere con otras operaciones de salvamento y ofrece información de gran utilidad.

Palabras clave: sonda XBT, oceanografía operacional, método inverso.

INTRODUCTION

A good knowledge of wind and ocean current velocity fields is the most relevant operational information needed for the search and rescue of shipwrecks or drifting objects, or for foreseeing the spread of waste and marine pollutants. In most cases, basic knowledge of in situ principal currents should improve efficient research strategies, in which time saving is the main objective. Under circumstances in which wind action is predominant, a simple model based on the wind-induced drift can provide reasonable forecasts of the motion of floating objects on the sea surface. However, in regions where the wind is not the only important mechanism in current generation, such as areas with strong frontal density currents (typically in the shelf-break transition), the spatial variation of the thermohaline vertical structure may contribute considerably to the sea surface velocity. Such information can be extracted either from specifically dedicated monitoring equipment (moored instruments, coastal radars, etc.) or from historical time series, which may provide reasonable predictions of marine currents for any situation combined with a forecast system.

Geostrophic balance has been widely used since the beginning of the twentieth century to assess the ocean's motion. This method is justified because the geostrophic equilibrium is a reasonable first approach to the ocean's state. The vertical thermohaline structure is presently a major issue in relation to techniques for assimilating data into numerical ocean models to provide acceptable realistic circulation schemes (Wilkin *et al.*, 2005). For operational purposes, the vertical thermohaline structure of the ocean can obviously be retrieved by directly measuring temperature and salinity through regular and continuous sampling using conductivity-temperature-depth (CTD) probes, arrays of moored instruments, etc. As an alternative, the vertical density field may still be obtained through historical data or dynamical relationships between related variables (geopotential height, sea level anomalies, etc.). Although international programmes (e.g. the Argo program, http://www.argo.ucsd.edu) are making a concerted effort to make uniform sampling strategies available, we are still far from a position equivalent to the meteorological network for weather forecasts. Marine emergencies require a spatial and temporal degree of resolution that is in most cases unattainable by operational systems. Additionally, numerical models used to optimise search and rescue strategies of drifting objects or to forecast oil dispersion from accidental releases have some deficiencies related to the lack of information of the ocean's state. For example, Lagrangian dispersion models are built taking into account a stochastic and a deterministic component, usually separated into several constituents to which both wind-induced drift and surface ocean currents make an important contribution (Montero *et al.*, 2003; Hackett, 2004; Carracedo *et al.*, 2006). If surface current observations are not available, the strategy is often to obtain them from a forecast system, which in turn includes again the wind forcing. Several model predictions carried out during the Prestige incident showed a faster dispersion of the oil spill over the Biscay Bay than the observations and failed to reproduce surface drifter observations (Carracedo *et al.*, 2006; Caballero *et al.*, 2008, and references therein). A better agreement was obtained when subsurface velocities (below the mixed layer) from a forecast model were extrapolated to the surface and then introduced into the dispersion model as the ocean current component (Daniel *et al.*, 2004). The added problem was that subsurface circulation was again not reliable due to the lack of observations to diagnose the initial conditions of the forecasting system.

Within the context of ocean research, it is evident that research vessels equipped with the appropriate instruments (CTD profilers and acoustic Doppler current profilers [ADCPs]) and/or new autonomous devices such as Argo floats or gliders may provide the three-dimensional density structure for a given region and measure ocean velocity fields directly. However, during a marine emergency this acquisition of data cannot be planned or quickly improvised. For this reason, it is necessary to develop simplified strategies aimed at obtaining a quick and efficient response during a marine emergency situation, taking into account the available resources (usually boats and/or helicopters). Here we describe a useful way to estimate the thermohaline structure from a set of expendable bathythermograph (XBT) profilers in combination with historical data. The operations and infrastructure needed match the above requirements and were tested in two operational training exercises carried out in May and November 2006 by the national Spanish office responsible for marine safety and rescue (SASEMAR, http://www.salvamentomaritimo.es). The data acquisition protocol during these exercises considered two main sam-

pling actions: the release of drifting buoys for tracking, validation and calibration of the oil dispersion model (Sotillo *et al.*, 2008), and a short cruise with XBT probes during the initial stage of the hypothetical accident.

With these two sets of data, estimation of the vertical thermohaline structure is reduced to estimating salinity profiles from temperature profiles. This problem has been studied over many years with the purpose of inferring the ocean velocity (Stommel, 1947; Emery, 1975; Hansen and Thacker, 1999, and references therein). Traditionally, marine technology has developed more accurate instruments for measuring temperature than salinity, so temperature is at present rather well sampled while salinity still remains an undersampled variable. As a consequence of this, recent attempts and schemes developed to retrieve the ocean salinity field are mainly based on measures of complementary variables (i.e. sea surface salinity, sea level anomalies [Sabia *et al.,* 2006]). The renewed interest in measuring salinity is due to its role in the Earth's climate, not only because it is an important component of the ocean's dynamics but also because it is a crucial variable for understanding the Earth's water cycle (Lagerloef *et al.*, 1995; Font *et al.*, 2004).

Here we present a methodology for recovering the salinity from temperature profiles by using climatological T-S curves. The paper is organised as follows: First we present a brief description of the field data collected during the training exercises (Section 2) and the analysis of existing historical data (Section 3). Section 4 describes the details of the methodology applied and Section 5 presents the results obtained during the salinity recovery and validation. Finally, Section 6 provides a summary and some conclusions.

FIELD EXPERIMENTS

In 1995, the International Maritime Organisation (IMO) approved the Oil Pollution Preparedness, Response and Co-operation (OPRC) agreement establishing recommendations in terms of maritime safety and accidental pollution at sea. The signatory States were urged to carry out training exercises that involved facing possible marine emergencies. As part of this agreement SASEMAR organised two exercises off the northwest coast of Spain in May and November 2006, GIJON-2006 and FINISTERRE-2006, respectively. During these exercises a technical unit (USyP) was set up to provide forecast and data analysis to assess the management operations (Sotillo *et al.*, 2008). The USyP is a contribution of the ESEOO project (http://www.eseoo.org) with the goal of providing an oceanographic operational system ready to respond immediately to marine emergencies (Álvarez *et al.*, 2007). The main tasks attributed to this unit concern the specific forecasts of ocean and meteorological conditions in the area, including an oil spill dispersion model (Castanedo *et al.*, 2006, Model TESEO). Additionally, the unit is tasked with advising the authorities on the acquisition of new data necessary to improve the forecasts.

During the exercises presented here the USyP proposed compiling temperature profiles to characterise the hydrographic conditions in the area by means of expendable probes (i.e. XBTs). The goal was to evaluate the feasibility of undertaking a rapid field sampling within the operations of rescue and safety, which constitute the primary missions of SASEMAR during an emergency. The sampling was carried out on board Salvamar, a relatively small regular rescue boat 20 m in length. This led us to adapt the manufacturer's XBT desk system to be able to work autonomously not only on research vessels but also on opportunity vessels. The main problem in fulfilling this requirement was the power supply. In order to bypass it, we prepared an optional battery pack with all the voltages required by aerial amphenol connectors (Fig. 1a).

The operator can thus decide whether to connect the system to the ship's power supply (220 V / 50 Hz) or to the battery pack. These modifications allow the system to be carried on small boats with an earth wire (for boats with a non-metallic hull, an additional wire is needed to close the system). The whole package fits into two small rigid suitcases and is easy to install and deploy. The system battery autonomy is usually greater than the laptop battery autonomy, so the system is driven by the latter, and this is an important constraint on long (more than 3 h) deployments.

During their descent, XBT probes measure water temperature with a fast thermistor. A very thin copper wire transmits the temperature data to the computer, where it is recorded for later analysis. Each probe model has a maximum depth range associated with the length of the copper wire. The probes are built with a ballistic shape that ensures a constant falling velocity, so that the depth of the probe can

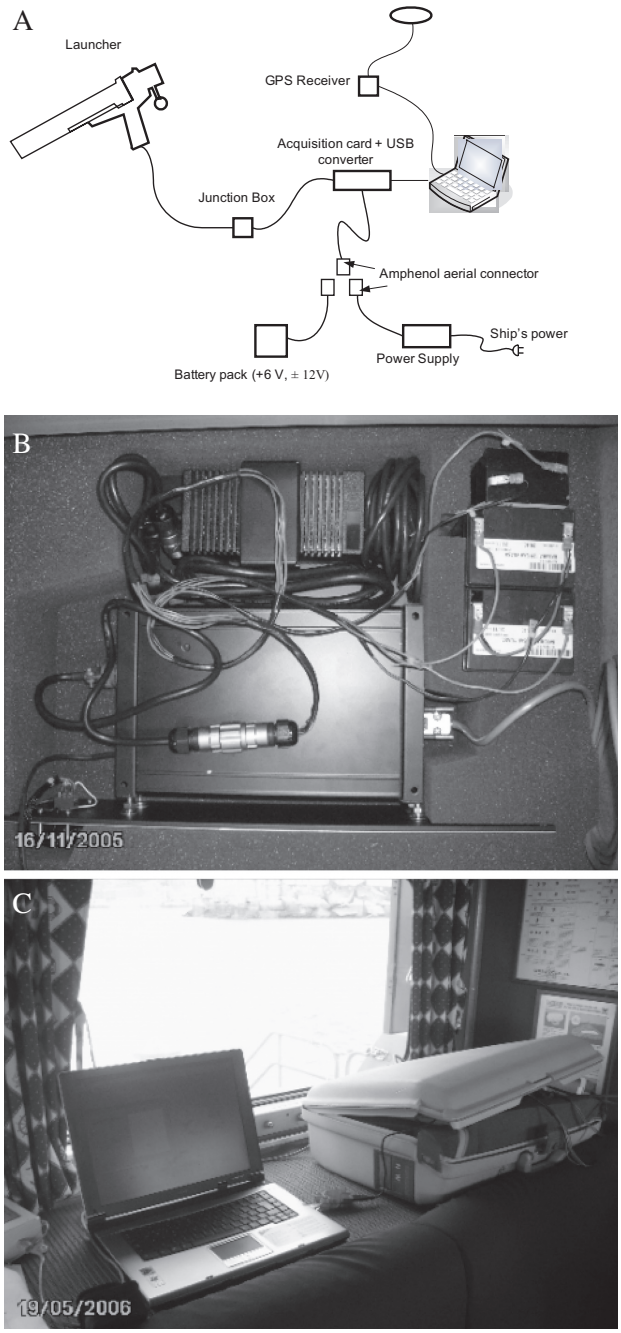

FIG. 1. – A, schematic diagram of the XBT acquisition system adapted to work autonomously; B, detail of the aerial amphenol connectors to the battery pack; C, the suitcase containing the desk system and the laptop used in the exercises.

be inferred from the time after deployment. Small boats do not often carry an acoustic system to survey deeper waters. This is important in the shelf/break area because if the maximum depth allowed by the probe is greater than the local topography then the probe continues measuring even after it has reached the bottom. This happened in our case with the T-10 model used for depths lower than 200 m and with the T-7 model used for depths lower than 760 m. In these cases, if the wire is not cut the profiles show almost constant values at the end of the profile. XBT data were pre-processed to correct such errors before being transmitted to the USyP.

In both samplings, model T-10 XBT probes (nominal maximum depth 200 m) were used for casts over the shelf while model T-7 probes were used for the shelf-break and interior ocean locations (nominal maximum depth 760 m). The probes are calibrated by the manufacturer. The model T-7 XBT probe is capable of a temperature accuracy of ±0.15ºC. The vertical resolution in both cases is 65 cm, which is considerably greater than the resolution needed for the present operational purposes.

GIJON-2006 Experiment

This exercise took place on May 22-25 2006. A hypothetical situation was considered, in which two ships collided off the north coast of Spain (43º40'N, 5º40'W), near the city of Gijón within the Bay of Biscay. The hypothetical emergency situation included the rescue of people as well as a fictitious spill of 159000 t of oil from a tanker.

Within the response actions, a rescue boat deployed several surface drifters to fix the spill. It also carried out a XBT sampling along two sections perpendicular to the coast, one directly crossing the accident location and one a few miles to the west (Fig. 2A), collecting 18 profiles in less than 5 hours. Additionally, not explicitly included in the response plans, the Spanish Institute of Oceanography (IEO) performed two standard oceanographic cruises for CTD sampling, simultaneous with the XBT sampling, aimed at gathering data for validation purposes. However, both cruises had to be postponed due to the rough weather conditions. They were finally carried out (ESEOO0506-I, ESEOO0506-II, Fig. 2A) a few days later (May 24-29) aboard the R/V José de Rioja, and covered a greater region around the location of the incident. Although both XBT sections were surrounded with the CTD sections nearly at the same locations and with a relatively small time delay, the dynamics of the oceanographic conditions evolved very rapidly during the exercise (Sotillo *et al.*, 2008).

FINISTERRE-2006 Experiment

A similar training exercise also simulating an accident with a tanker that produced an oil spill was

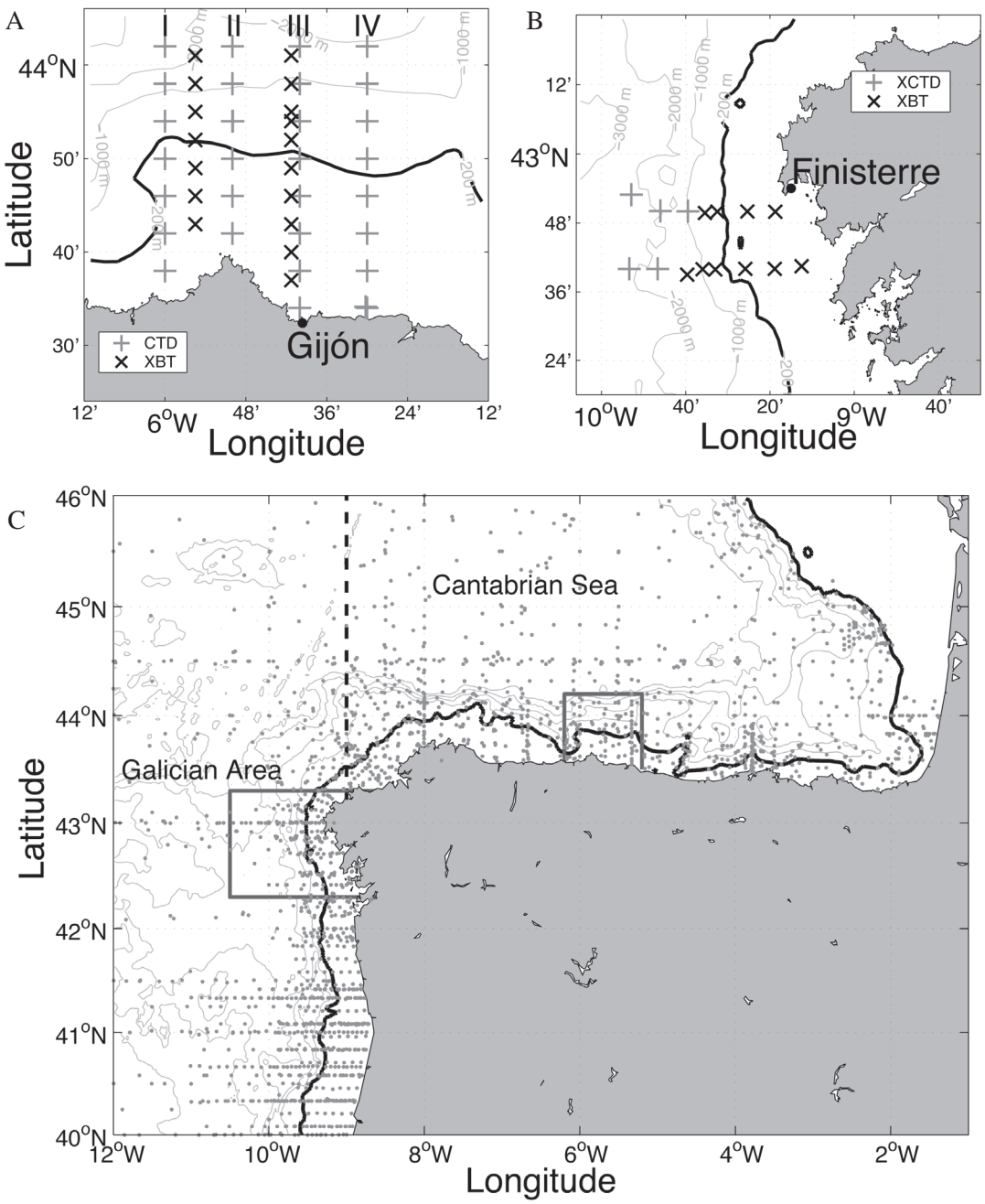

FIG. 2. – Oceanographic cruises during GIJON-2006 (A) and FINISTERRE-2006 (B) exercises. Sampling with XBTs, CTDs and XCTDs is indicated. Spatial distribution of the Hydrobase dataset in the region of interest (C). Exercise locations are bounded by a gray box. The thick solid line marks the isobath corresponding to 200 m. The meridional dashed line indicates the boundary between Galician Area and Cantabrian Sea.

planned around Galicia (42º40'N, 9º20'W) in November 2006. Two XBT sections were carried out over the shelf on November 14. In this case the casts at the end of the sections were covered with five XCTD probes, which provided the temperature and salinity in the water column with a vertical resolution of 0.1 m. Information from the XCTDs is used here to validate the salinity estimates obtained with the methodology presented in Section 4 (Fig. 2B).

HISTORICAL DATA

Dataset

In order to characterise *S–T* and *S–d* curves, we need historical data corresponding to the north and northwest area of the Spanish coast: the Bay of Biscay and the region of Galicia, respectively. Historical profiles were downloaded from the Hydrobase

database (http://www.whoi.edu/science/PO/hydrobase/). This data set integrates several databases, including the World Ocean Database 2001, the WOCE Hydrographic Programme, NSIDC (Joint US / Russian Atlas of the Arctic Ocean), ICES and BarKode (Barents and Kara Seas Oceanographic Database), all of which include data quality control flags. Profiles of conductivity, temperature and depth were downloaded in quality control mode. These profiles correspond to gridpoints 7400 and 7401 in WMO (World Meteorological Organisation) notation.

The domain selected to build the climatology was limited to 12-1ºW and 40-46ºN (Fig. 2C). The coastal area in this region is affected by a relatively large number of rivers, producing significant water variability over the shelf due to the fresh water plumes (Ruiz-Villarreal *et al.*, 2006). We divided the whole domain into two areas, the Galician Area and the Cantabrian Sea, separated by the meridian 9ºW. We thus have two regions with different oceanographic conditions on each side. The geographic distribution of the profiles shows that many profiles in the Cantabrian Sea are close to the area of Santander (43º27'N, 3º49'W), regularly sampled throughout the year (Fig. 2). In the Cantabrian Sea the data cover both the shelf area and the interior ocean rather well up to nearly 100 km offshore. In the Galician Area there also appears to be a good coverage over the shelf break, while the interior ocean has been less sampled, particularly in front of the Galicia region.

Water masses

Figure 3 presents *S*–*T* and *S*–*d* relationships made with historical observations from the Galician Area and the Cantabrian Sea. The interface between central and intermediate water masses is indicated by the isoline corresponding to σ_θ=27.25, located within the salinity minimum (van Aken, 2000; González-Pola *et al.*, 2005). In both cases we have superim-

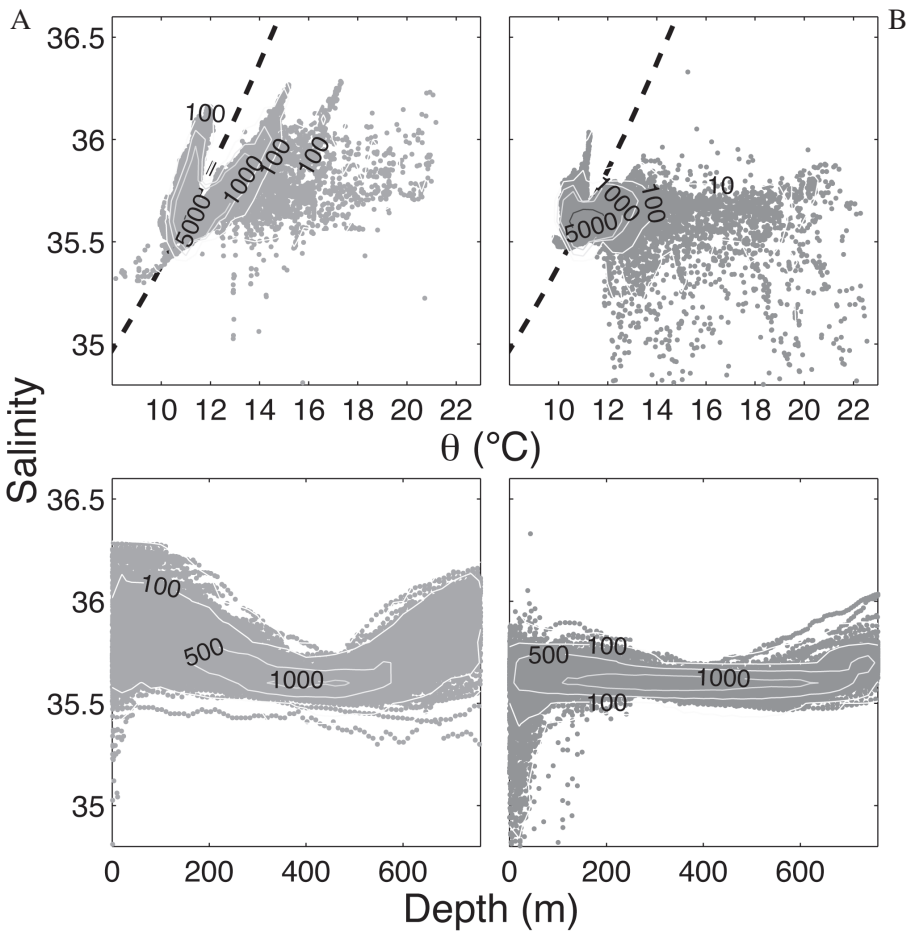

FIG. 3. – *S*–θ (upper) and *S*–*d* (lower) relationships in the Galician Area (A) and Cantabrian Sea (B). σ_θ=27.25 is shown. Contours indicate the density of observations (obs ºC).

posed the density of observations (*DO*), defined as the number of observations available in each square whose sides are one unit in temperature and in salinity. *DO* may help to describe the relative importance of water masses in the *S–T* and *S–d* planes. At central levels in the Galician Area (Fig. 3A), Eastern North Atlantic Central Water (ENACW) of subtropical origin (ENACWst) is observed as a rather straight line from (11ºC, 35.6) to (14ºC, 36) (Fiúza and Halpern, 1982; Ríos *et al.*, 1992; Pérez *et al.*, 1995), and a *DO* typically higher than 1000 obs ºC^{-1}. At intermediate levels we observe a salinity minimum probably related to the influence of Sub-Arctic Intermediate Water (SAIW, van Aken [2000]); the dominant water mass at this level is Mediterranean Water (MW), with a clear salinity maximum at (11.7ºC, 36.2) and a *DO* higher than 1000 obs ºC^{-1}. Water masses in the Cantabrian Sea (Fig. 3B) are rather similar to those of the Galician Area, though with a different contribution and composition. In this case, ENACW has a subpolar origin (ENACWsp), where the relatively high temperature and salinities at the surface have disappeared (Harvey, 1982; Ríos *et al.*, 1992; Pérez *et al.*, 1995). The geographical distribution of water masses at central levels in the north-northwest of Spain is clearly illustrated by Ríos *et al.* (1992) (their Fig. 12), with ENACWsp dominating in the Cantabrian Sea and ENACWst doing so in the Galician Area. At intermediate levels the minimum in salinity has disappeared and the presence of MW is lower than in the Galician Area. (For a detailed description of the water masses at central and intermediate levels in these regions, the reader is referred to Pérez *et al.* (1995), van Aken (2000, 2001), González-Pola *et al.* (2005) and references therein).

Analysis of historical data

The analysis of historical data was performed by separating the data set into continental shelf and interior ocean regions, defined by depths shallower and deeper than the 200 m isobath, respectively, as recommended by previous research (Siedler and Stramma, 1983; Marrero-Díaz, 2002; Marrero-Díaz *et al.*, 2006).

Interior Ocean

The historical profiles for the interior ocean region were cut to 760 m depth because this is the maximum depth cast by the deepest XBT model. In order to get an idea of the representativeness of the database, we show the spatial and temporal distribution of profiles (Figs. 2C and 4A). There was a considerable number of profiles in the 1970s, falling sharply in the period 1975-1980 and rising again until 1998. The number of profiles taken per month and zone are summarised in Table 1 and Fig. 4A (lower). A certain concentration of profiles appears towards the summer, particularly between March and September, although there is a significant amount in December and January in the Galician Area (see Fig. 4A). Both zones show a clear maximum in the spring and summer seasons. When data for all months are merged, the gaps are filled, showing a rather good distribution in both areas with 793 and 727 casts in the Cantabrian Sea and Galician Area, respectively (see Table 1 and Fig. 4A).

In Figure 5 we have represented the monthly variability of temperature and salinity observations for both regions. In the Galician Area the T-S dispersion is similar to that described in Figure 3, with ENACW dominating at central levels and MW at intermediate levels. This schema is particularly evident in winter months, in contrast with the summer months, when the insolation induces higher temperatures at the surface, rising from 14ºC in February to near 22ºC in August. The runoff from rivers in Galicia affects the upper ocean observations from March to May. At intermediate levels, MW can be observed throughout the year, and from June to October intermediate waters with minimum values of salinity can be observed, probably related to SAIW. The description of the water masses in the Cantabrian Sea also fits the description given in Figure 3, with ENACW dominating at central levels throughout the year; the

TABLE 1. – Monthly distribution of number of profiles and measurements (normalised by the total data set shown in the bottom row) in the interior ocean/continental shelf within the Galician Area and Cantabrian Sea.

	Galician Area		Cantabrian Sea	
	Profiles	Measurements	Profiles	Measurements
January	4.3/3.7	3.9/3.6	11.1/6.0	11.9/6.5
February	1.8/3.2	1.3/3.1	1.4/0.0	1.5/0.0
March	11.6/11.6	15.3/12.6	7.6/7.2	7.5/7.6
April	23.7/30.5	23.5/30.4	32.3/36.9	32.2/37.4
May	13.9/18.5	10.9/17.1	9.6/15.6	8.7/14.2
June	5.7/6.4	4.2/7.0	3.9/0.0	3.6/0.0
July	9.7/5.0	8.7/5.3	8.4/10.3	8.1/9.7
August	13.2/4.7	15.6/4.8	7.2/0.0	6.7/0.0
September	4.7/2.7	5.1/2.6	4.5/3.5	5.8/4.0
October	6.0/4.2	6.4/4.4	2.9/2.2	3.1/2.0
November	3.0/5.5	3.0/5.2	2.3/2.4	23.5/2.0
December	2.4/4.0	2.2/4.1	8.8/15.3	8.5/16.0
Total dataset	793/622	57895/9305	727/544	53086/7932

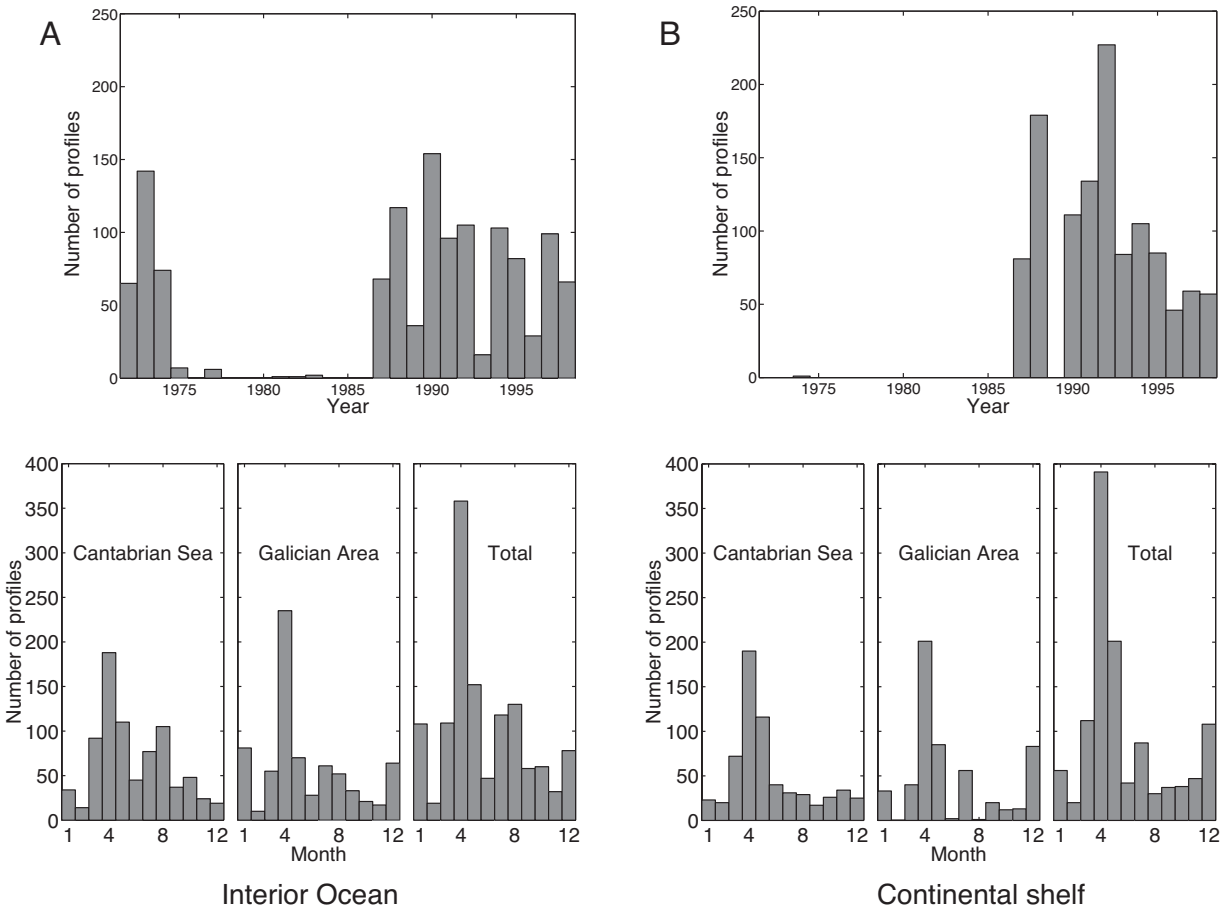

FIG. 4. – Yearly (upper) and monthly (lower) distribution of CTD profiles available for the interior ocean (A) and the continental shelf region (B). Monthly distributions are given for the Cantabrian Sea (left), Galician Area (middle), and total (right). See also Table 1.

insolation effect is detected in summer, with maximum surface temperature reaching up to 22ºC in August. The effect of river runoff is clear in this case from November to June, with relatively low salinities at the surface. At intermediate levels, the presence of MW is irregular, with values notably lower than those described for the Galician Area.

Continental shelf

After the 1970s, the greatest number of profiles measured on the shelf area took place during the 1990s, with 60 to 80 profiles per year (Fig. 4B, upper). There are about 10-20 profiles per month except during spring (March, April and May), where the number rises to between 100 and 200 profiles (Fig. 4b). In February, June and August in the Galician Area the number of profiles is very scarce or inexistent. When we group all the data together we have a rather regular coverage of the regions, with 622 and 544 profiles in the Galician Area and Cantabrian Sea, respectively (Table 1).

T-S diagrams for observations on the continental shelf do not exhibit great differences between the two areas (Fig. 6). There is a clear vertical development between June to October related to the summer warming, while in the winter months a clear signal appears, corresponding to fresh water discharges from rivers, with minimums of sea surface salinity between November and May.

As a result, we will consider here a seasonal criteria based on two groups that we will generically call winter-like (from October to March) and summer-like (from April to September) seasons. This separation is in agreement with the poleward and equatorward slope mean flow regimes depicted from surface drifter observations in the Bay of Biscay (van Aken, 2002).

POLYNOMIAL FIT

The good correlation between temperature and salinity in the ocean have led oceanographers to

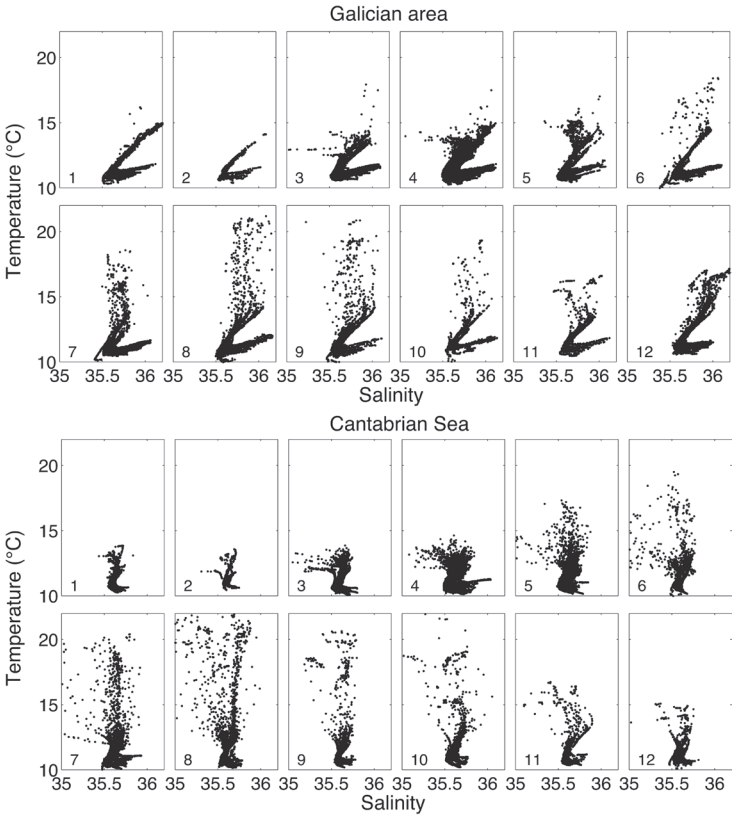

FIG. 5. – Monthly TS diagrams for the interior ocean corresponding to the Galician Area (upper) and Cantabrian Sea (lower).

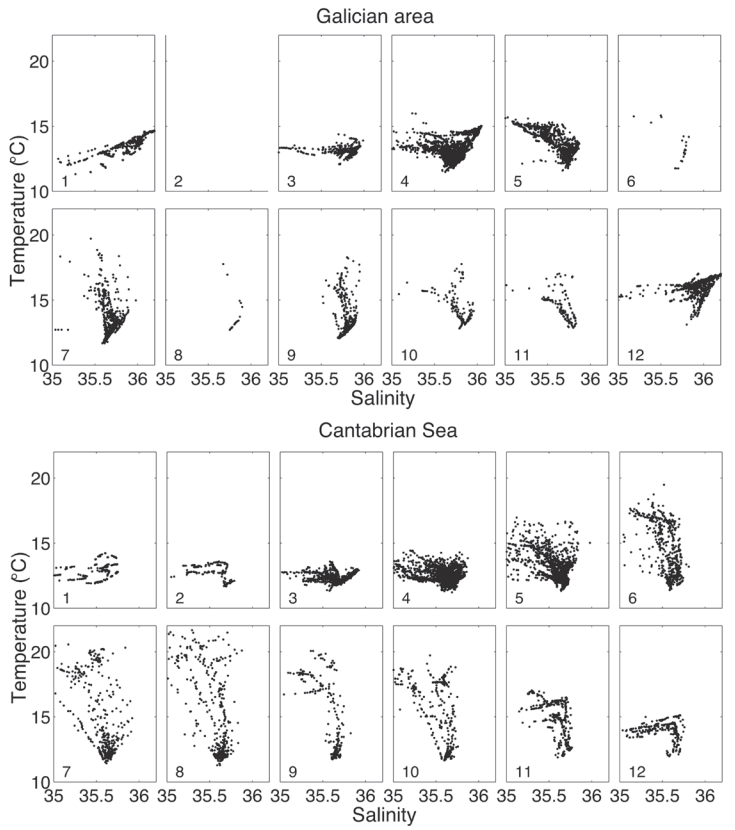

FIG. 6. – Monthly TS diagrams for the continental shelf area corresponding to the Galician Area (upper) and Cantabrian Sea (lower).

establish formal relationships that could eventually help to calculate one as a function of the other. Temperature has been widely measured in the ocean with a higher frequency than salinity, so this last variable is generally calculated as a function of temperature (Stommel, 1947; Flierl, 1978; Emery and Dewar, 1982; Siedler and Stramma, 1983; Kessler and Taft, 1987; Marrero-Díaz *et al.*, 2001). Siedler and Stramma (1983) tested the relationship that showed the best performance to estimate geopotential anomalies in the eastern North Atlantic, in the absence of salinity observations. They tried several possibilities, considering that salinity could be estimated from temperature or from both temperature and pressure. In general, they obtained the best results when geopotential anomalies were estimated with the salinity as a function of temperature; however, in those regions close to the Iberian Peninsula where MW was clearly observed at intermediate levels, results were improved when the pressure was considered in the system. As discussed in the previous section, MW is observed in the historical data analysed here, so we need a dependence of salinity on depth, beyond the dependence on temperature. The fitting procedure proposed here is an extension of that developed by Marrero-Díaz *et al.* (2006), in which a polynomial adjustment for salinity as a function of both temperature and depth is suggested as follows:

$$S = a_0 + a_1(T - T_r) + a_2(T - T_r)^2 + \cdots + a_n(T - T_r)^n + \\ + b_1(d - d_r) + b_2(d - d_r)^2 + \cdots + b_m(d - d_r)^m + \varepsilon \quad (1)$$

Considering the total number of data, N, we can rewrite the proposed model (1) in a compact way as

$$S = E^T A + \varepsilon \quad (2)$$

where E^T is the transposed $(n+m+1)\times N$ elements matrix state whose columns are formed by $[1, T_i, T_i^2, \ldots, T_i^n, d_i, d_i^2, \ldots, d_i^m]$, $(i=1,N)$, and A is the $(n+m+1)$ vector of coefficients $A = [a_0, a_1, \ldots, a_n, b_1, b_2, \ldots, b_m]$. ε is related to the model's inefficiency in explaining the variability in the observations. Instead of using the absolute values of T and d we work with anomalies with respect to reference values, T_r and d_r; by doing so, the y-axis offset corresponds to the salinity where $T=T_r$ and $d=d_r$, instead of obtaining any arbitrary values for the set of coefficients. We locate this reference in the interface between central and intermediate waters, where a minimum in the salinity dispersion is observed (Fig. 3). Thus, reference salinity is 35.6, and T_r and d_r are determined for that salinity value from the historical data, obtaining T_r=11ºC and d_r=400 m.

The set of equations (2) constitutes a grossly overdetermined system and its solution may be obtained by a fit in a least-squares sense. A weighted and tapered least squares adjustment was applied to minimise both the residuals and the size of the unknowns (Menke, 1984). The solution is obtained after minimising a cost function, J, written as

$$J = \varepsilon^T Rnn^{-1} \varepsilon + A^T Rxx^{-1} A \quad (3)$$

where Rnn and Rxx are weighting matrices. Weights incorporate *a priori* physical information related to observations statistics crucial to better conditioning the solution estimate. The covariance of the residuals, Rnn, is *a priori* related to the uncertainty in determining S with the suggested polynomial relationship, so we choose Rnn as a matrix whose main diagonal is filled with the variance of the historically observed S at each depth level. For the covariance of the unknowns, Rxx, we normalise by the variance of each column of E, so that all unknowns have the same importance in the system:

$$Rxx = diag(std(E)^2) \quad (4)$$
$$Rnn = diag(std(S)^2) \quad (5)$$

where *std* is the standard deviation, *diag*() converts to a matrix with non-zero numbers in its main diagonal the outcome from the inside parenthesis, and S contains the whole salinity array.

Figure 3 shows the relationship between the independent variable (S) and the dependent ones (T and d) in the Galician Area and Cantabrian Sea. An inspection of these panels may help to make a first guess of an expected dependence between S, T and d. In the upper panels, salinity shows a clear minimum. S decreases from 36.1 to 35.5 as temperature increases, then increases roughly to 35.9 before finally decreasing to around 35.6 in the upper layers, which are highly variable. In the lower panels, salinity increases with depth from 35.7 at the sea surface to 35.9 at 150 m depth, then decreases to 35.6 at 400 m and finally increases to 35.8 at 760 m depth. A clear minimum is always present in both panels and a curvature change is also appreciated. In the S–d plane this behaviour is more evident for the Cantabrian than for the Galician region (Fig. 3c,d). Thus, a cubic polynomial functional relationship $S(T,d)$ seems

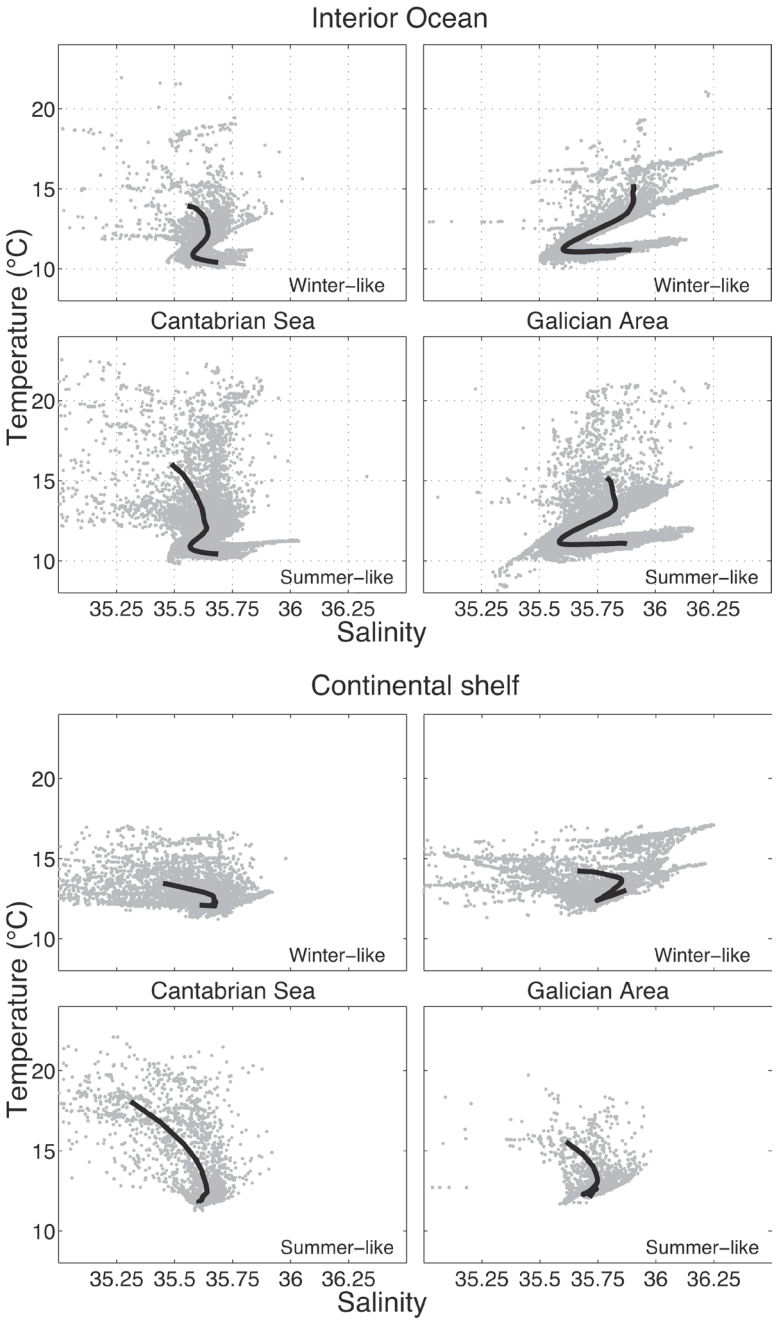

FIG. 7. – Upper: averaged temperature and salinity profiles for each region and temporal season in the interior ocean, as indicated in the text. Lower: same as before, but on the continental shelf. Gray dots represent the observations grouped for each case.

to be rather coherent with this geometrical description.

In order to have a more consistent and objective way to determine the final degrees for T and d in the polynomial relationship, we applied an ANOVA test. We tried several polynomial fits in which n and m were systematically varied from 0 to 9, calculating for each case the corresponding simulated salinity. The ANOVA test indicates that the total variability in the salinity (TVS) can be evaluated as the sum of the variability between simulations (VBS) plus the variability within each simulation (VWS). In other words, we are interested in assessing how much of the total variability is explained by each case considered, so we discuss our decision in terms of a quantity R_a^2, defined as the ratio between the variability explained by each simulation and the total variability:

$$R_a^2\left(n,m\right)=\frac{VBS\,N-1}{TVS\,K-1} \qquad (6)$$

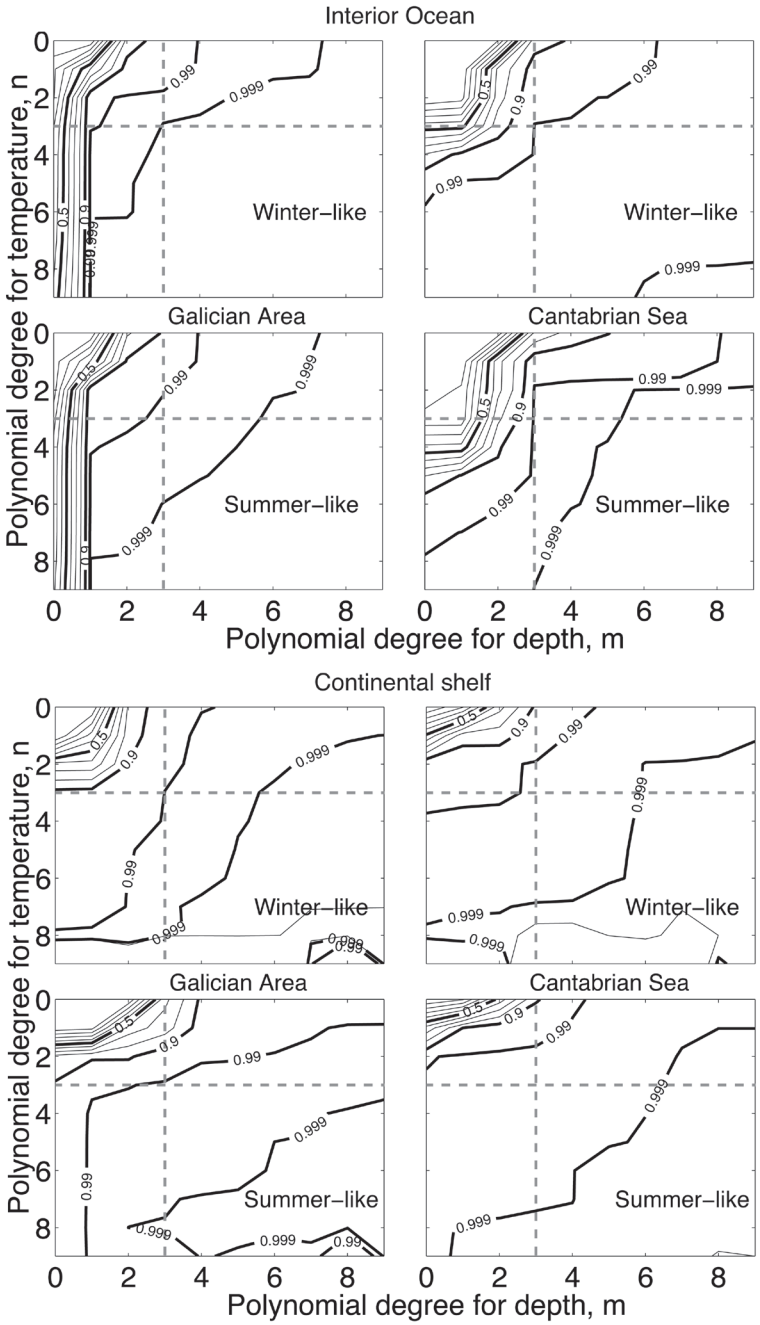

FIG. 8. – Upper: R2a contour lines for Galician Area and Cantabrian Sea corresponding to the winter-like and summer-like seasons in the interior ocean, as a function of polynomial degrees. Lower: same as before, but on the continental shelf. Gray dashed lines indicate the degrees of the polynomial fit finally used.

where n and m are the polynomial degrees, N is the number of observations and K is the number of cases considered.

In order to perform the ANOVA test, we use T, d and S averaged for each region and season, in the interior ocean and in the continental shelf. Figure 7 shows the T-S diagrams for the data joined for each case, with the average profiles superimposed. The distribution of R_a^2 as a function of m and n for each season and region is presented in Figure 8. R_a^2 indicates that either T or d alone can explain on their own (m=0 or n=0) a relatively high amount of the variability in S by just increasing their respective degrees above 5 or 6 (except for the Galician Area in the interior ocean, where T does a poor job alone). However, when we combine both variables (n>0 and m>0), R_a^2 reaches high values with relatively low m and n values. Notice that for m=n=3 a lower boundary of 99% of explained variability is fulfilled for all cases. This confirms our first guess from geometrical

inspection of the *T–S* and *S–d* distributions. Higher degrees do not provide any substantial improvement of the fitting.

The matrix state *E* consists of 25000×7 observations in each zone and for each season. This implies a covariance matrix *Rnn* with a size of 25000×25000 (around 5 Gb of memory) whose inversion is very expensive computationally. In order to solve this, we divide the whole database into random subsets of observations to compute for each group their corresponding coefficients. For each subset the statistics are still robust enough to expect not much variation in the estimated values of the coefficients. The method is validated with data from February and September in both zones, which are sufficient to deal with the inversion considering four subsets. Table 2 compiles the coefficients obtained using the whole data set and those coefficients obtained by averaging coefficients calculated from the subsets. The similarity for both types of coefficients can be observed, in general differing in the third decimal. In addition, it is interesting to note that the discrepancy diminishes when the number of available observations increases, in such a way that for September, which is the month with the largest number of observations, the results are very similar for both cases.

Coefficients obtained for the winter-like and summer-like seasons in the Galician Area and Cantabrian Sea for the interior ocean and continental shelf areas are listed in Table 3. In general, coefficient values are quite stable in all cases, the main differences being found in the comparison of those estimated in the interior ocean with those over the continental shelf. The stability in the coefficients from zone to zone and from season to season is one of the most important properties of our solution, because it indicates that the coefficients are responding to variability in observations instead of to a mathematical artifact. The polynomial coefficients are significant in practically all cases (their uncertainties are always lower than their value), having a higher uncertainty over the continental shelf than in the interior ocean.

TABLE 2. – Coefficients estimated with the whole data set and averaging from subsets within the Galician Area (G) and Cantabrian Sea (C). Months and number of available observations are indicated. Coefficients considered are a_0, a_1, a_2, a_3, b_1, b_2 and b_3. Note that the third coefficient is multiplied by 10^3, the fourth by 10^2, the fifth by 10^3, the sixth by 10^4 and the seventh by 10^8.

Zone	Month	N.obs.	Full	Average
G	Feb	788	35.59±0.00	35.58±0.00
			0.03±0.01	0.03±0.01
			-48.00±9.30	-47.90±13.50
			1.83±0.39	1.82±0.57
			-0.11±0.02	-0.12±0.03
			0.01±0.00	0.01±0.00
			0.21±0.02	0.21±0.02
C	Feb	844	35.57±0.00	35.57±0.00
			0.12±0.01	0.12±0.02
			-13.20±13.30	-12.70±1.90
			0.82±0.37	0.82±0.52
			0.03±0.03	0.03±0.04
			0.01±0.00	0.01±0.00
			0.29±0.03	0.29±0.05
G	Sep	3112	35.58±0.00	35.58±0.00
			0.06±0.00	0.06±0.00
			-12.70±2.90	-12.60±1.70
			0.06±0.03	0.06±0.02
			-0.04±0.01	-0.04±0.01
			0.01±0.00	0.01±0.00
			0.20±0.02	0.20±0.01
C	Sep	3266	35.57±0.00	35.58±0.00
			0.14±0.00	0.06±0.00
			-25.30±2.00	-25.00±3.40
			0.14±0.02	0.14±0.03
			0.08±0.01	0.08±0.03
			0.01±0.00	0.01±0.00
			0.23±0.02	0.24±0.04

RESULTS AND VALIDATION

The application of expression (1) is used to recover the salinity for the XBT casts in the GIJON-2006 and FINISTERRE-2006 exercises. Coefficient validation is performed against independent data acquired during these exercises, so it is not included in the fitting procedure. The independent database used for validation is quite complete since it covers both the Galician Area and the Cantabrian Sea, both seasons (winter-like and summer-like), the interior ocean in both areas and some stations over the continental shelf during the GIJON-2006 exercise.

GIJON-2006 exercise

During the GIJON-2006 cruise, and after the XBT deployments, a quick visualisation of the raw XBT sections allowed us to identify the vertical stratification and the presence of a horizontal thermal gradient transverse to the shelf (not shown). As previously noted, the temperature profiles from a certain depth appear rather constant, especially at the shelf and shelf-break. Given that the XBT probes compute depth through the falling time, it is probable that the probe reached the floor at a depth lower than its standard range and it continued providing data. To solve this we take as a reference the temperature profiles of the closest CTD.

TABLE 3. – Polynomial coefficients obtained to retrieve salinity as a function of temperature and depth in the Galician Area (G) and Cantabrian Sea (C) during winter-like and summer-like seasons in the interior ocean and continental shelf.

Zone	Month	N.obs.	Coefficients	Open Ocean	Continental Shelf
G	Winter	19719/6658	a_0	35.54±2.828e-3	38.55±6.97e-1
			a_1	1.84e-1±6.349e-3	2.88e-1±3.93e-2
			a_2	-1.66e-2±3.022e-3	-6.43e-2±1.30e-2
			a_3	1.37e-4±3.51e-4	5 .91e-3±1.31e-3
			b_1	3.08e-4±2.462e-5	3.50e-2±7.12e-3
			b_2	1.54e-6±6.262e-8	1.31e-4±2.39e-5
			b_3	2.32e-9±2.934e-10	1.62e-7±2.62e-8
G	Summer	36447/1228	a_0	35.54±2.17e-3	38.40±5.06e-1
			a_1	1.77e-1±5.73e-3	3.71e-1±2.36e-2
			a_2	-1.76e-2±2.63e-3	-8.25e-2±7.66e-3
			a_3	1.37e-4±2.67e-4	6.10e-3±7.42e-4
			b_1	3.49e-4±2.30e-5	3.58e-2±5.337e-3
			b_2	1.46e-6±6.63e-8	1.29e-4±1.31e-5
			b_3	2.28e-9±2.83e-10	1.73e-7±2.10e-8
C	Winter	19623/7090	a_0	35.59±1.06e-3	38.57±3.60e-1
			a_1	6.07e-2±3.89e-3	1.22e-1±1.98e-2
			a_2	-1.31e-2±2.10e-3	-4.97e-2±8.69e-3
			a_3	6.43e-4±2.58e-4	5.52e-3±1.09e-3
			b_1	-3.89e-5±1.20e-5	3.41e-2±3.78e-3
			b_2	5.73e-7±2.65e-8	1.29e-4±1.31e-5
			b_3	2.28e-9±1.11e-10	1.59e-7±1.48e-8
C	Summer	41473/1777	a_0	35.57±1.16e-3	38.32±4.329e-1
			a_1	8.64e-2±4.55e-3	5.46e-2±1.01e-2
			a_2	-1.78e-2±2.59e-3	-5.27e-3±2.90e-3
			a_3	7.52e-4±2.74e-4	-4.32e-4±2.36e-4
			b_1	1.90e-5±1.51e-5	3.14e-2±4.57e-3
			b_2	6.85e-7±3.50e-8	1.18e-4±1.59e-5
			b_3	2.39e-9±1.60e-10	1.45e-7±1.83e-8

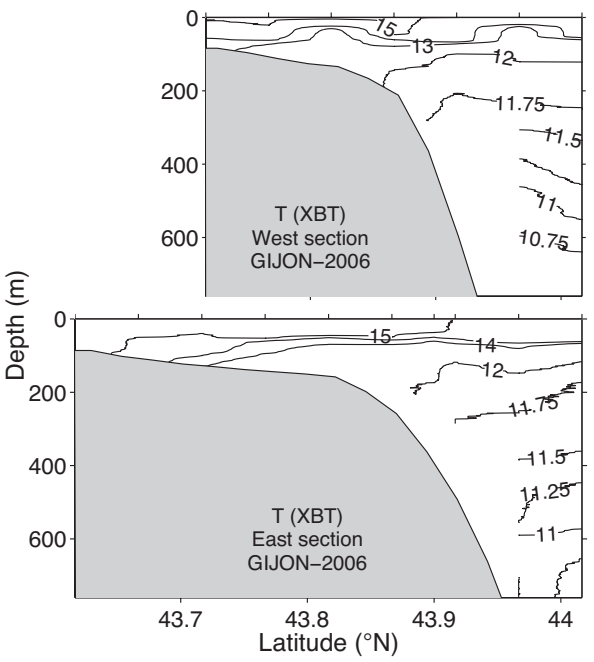

FIG. 9. – Vertical sections of temperature (ºC) measured by XBTs during the GIJON-2006 field exercise in the western and eastern sections.

In Figure 9 the cross-sections are represented according to this criteria, where the presence of a thermal front around the central part of the shelf-slope can be appreciated with its associated frontal current along the slope towards the east (flowing outside the figure). Surface temperatures measured by XBTs are nearly 15ºC, a value in good agreement with the historical data shown in Figure 5 during May; at intermediate levels, temperature is of the same order as that shown in the historical data (10-11ºC), with a slight influence of the MW. In order to compare XBT and CTD data, Figure 10 shows the corresponding temperature transects from the ESEOO0506-I cruise. It can be appreciated that observations from the two cruises are very similar in absolute values as well as spatial distribution, although the sections were not sampled exactly at the same points, the CTD section being much more precise and exhaustive in the vertical.

The historical database is classified by months and seasons, with data over the continental shelf and in the interior ocean. Monthly data are probably more informative than seasonal data, but they contain a considerably lower number of observations, which makes them less reliable. Hence, we considered four different strategies for validating the polynomial coefficients obtained in order to assess whether monthly variability is better reproduced than the seasonal

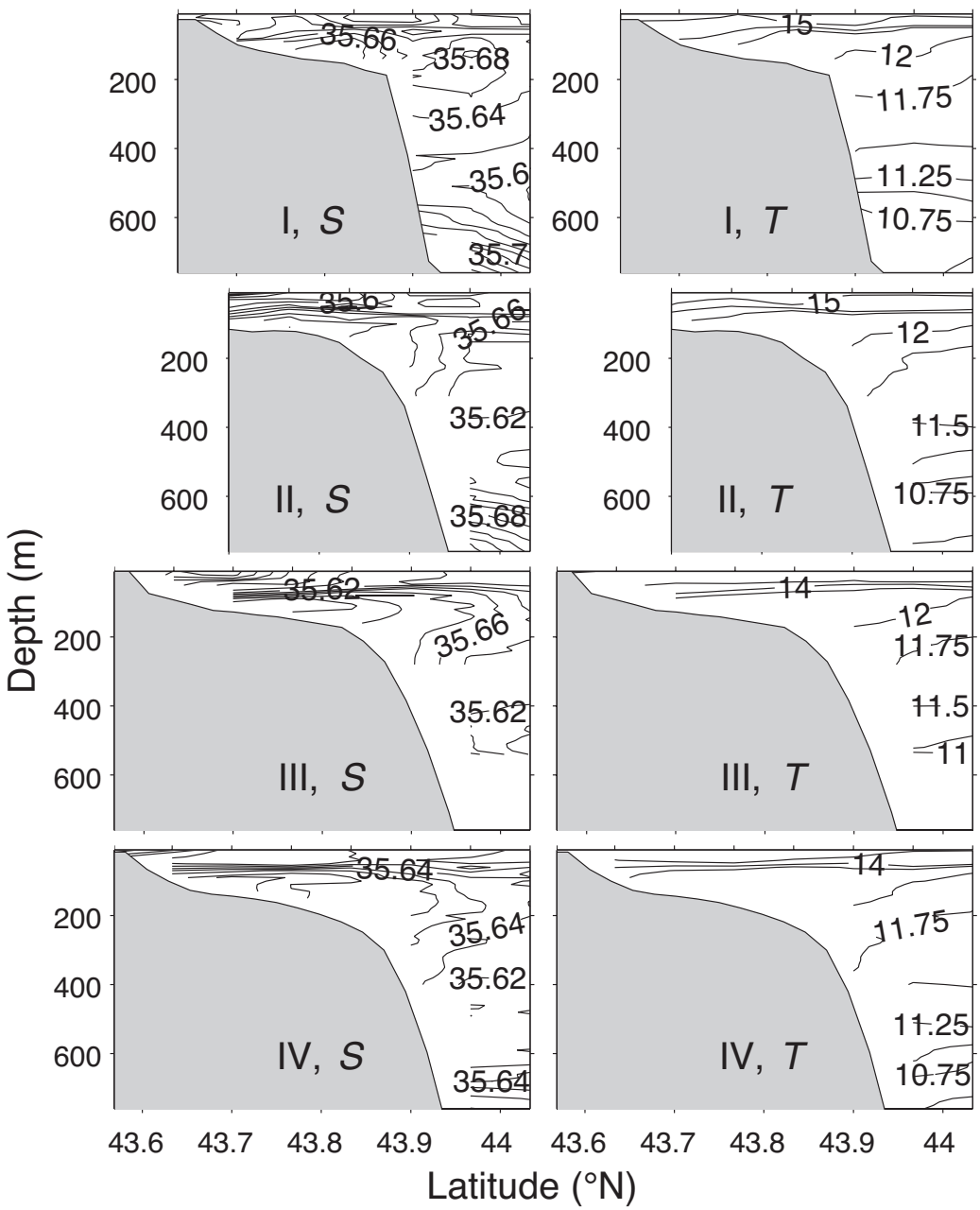

FIG. 10. – Salinity (*S*, left) and temperature (*T*, right) vertical sections during the ESEOO0506-I cruise as a function of latitude. Sections are numbered from west (upper row) to east (lower row) as shown in Figure 2A.

one and whether the separation criterion between the interior ocean and continental shelf is really important for estimating the coefficients. The four cases finally selected are:

Case *M*: retrieving salinity with coefficients estimated from historical data of the same *month* (in this exercise, during May). This first case comprises 48 different sets of coefficients: 12 months, 2 areas (Galician and Cantabrian) and 2 regions (interior ocean and continental shelf).

Case *Ss*: retrieving salinity with coefficients estimated from historical data corresponding to the same *season* (in this exercise, during winter-like). This case contains 8 different sets of coefficients: 2 seasons (winter-like and summer-like), 2 areas and 2 regions.

Case *M–IO*: retrieving salinity from historical data from the same *month for the interior ocean* area, also applied to the continental shelf area. This case compiles 24 sets of coefficients: 12 months and two areas.

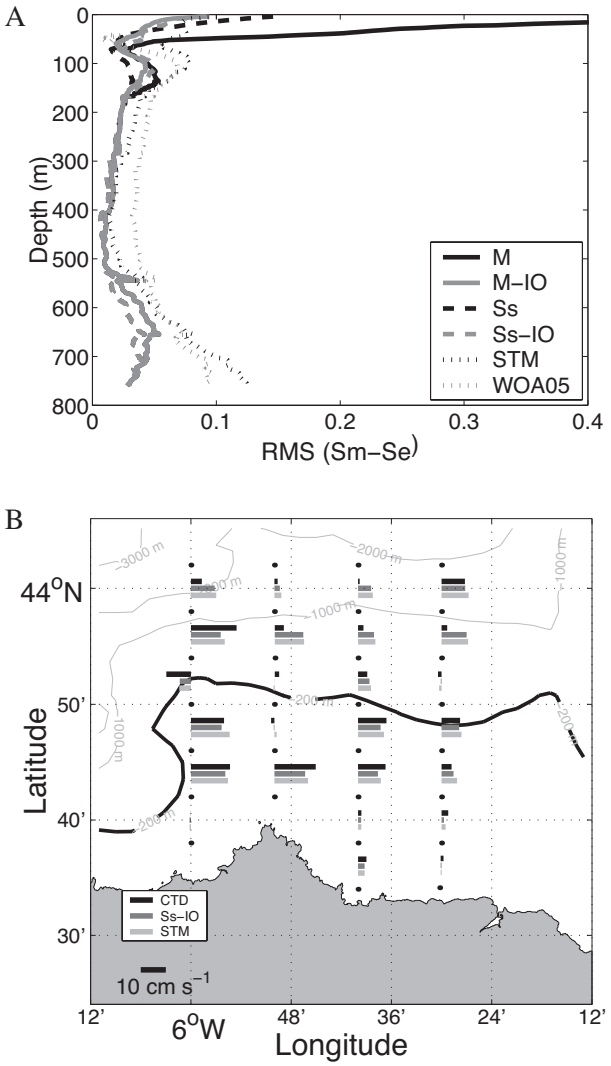

FIG. 11. – A, rms of the difference between measured and estimated salinity for six cases indicated in the legend (see text for details); B, surface geostrophic velocity during the GIJON-2006 exercise estimated with the CTD data, with our best polynomial coefficients (*Ss–IO*) and with STM case.

Case *Ss–IO*: retrieving salinity from historical data in the same *season for the interior ocean*, also applied to the continental shelf area. This case contains 4 sets of coefficients: 2 seasons and 2 areas.

Additionally, we also estimate the salinity following two alternative methods. The first method, suggested by Stommel (1947) (hereafter *STM*), simply takes the salinity as the depth-averaged salinity value from the historical data. The second method extracts the salinity from climatological salinity data at the closest grid point in the World Ocean Atlas 05 (*WOA05*, Locarnini *et al.*, 2006; Antonov *et al.*, 2006). The goodness of each case is evaluated by comparing the measured salinity in the CTD data during the ESEOO0506-I cruise with that estimated with the six methods (four polynomial fits, *STM* and *WOA05*). Figure 11A represents the average profile of the root-mean-square (rms) differences between the estimated and the measured salinity during the ESEOO0506-I cruise, applying the six cases. In general, the difference is lower than 0.05, with the highest deviations at the near-surface and at depths higher than 500 m.

In the upper 200 m it can be observed that salinity data deviate considerably in case *M*, probably because the historical dataset, with a relatively low number of observations during this month, does not represent the whole variability expected for this month. When we consider the polynomial coefficients obtained with historical data for the whole season (*Ss*), the results clearly improve in the upper 200 m. In the *M–IO* case, when we apply the shelf data coefficients estimated from the interior ocean corresponding to May, the result is again improved in the upper waters, which means that coefficients estimated with the historical data over the continental shelf do a poor job in retrieving the salinity for those stations. Finally, when we apply coefficients obtained with historical data from winter (*Ss–IO*), the results on the shelf are slightly worse than *M–IO*, but again considerably better than case *Ss*. *STM* and *WOA05* show a result of the same order as *M–IO* and *Ss–IO* close to the sea surface, though clearly worse than all cases in the rest of the upper 200 m.

Below 200 m, the differences between all methods diminish (Fig. 11A). However, *M* offers the same results as *M–IO*, while *Ss* does the same as *Ss–IO*, with rms values around 0.02. *STM* shows slightly higher rms deviations, while the worst case is the salinity estimated with the *WOA05* climatology. Below 500 m depth, where the dominant water mass is MW, the deviations increase to 0.05 for polynomial cases, while *STM* and *WOA05* doubles this deviation up to 0.1. A different approach is used by Thacker (2007), where polynomial fits are performed at selected depths. Their deviations are very similar to the one obtained here with the best case (*Ss–IO*) in the upper 500 m.

In order to have a much more global idea of the performance of the different cases, we also estimated a depth-average of the rms difference between estimated and measured salinity (see Table 4). In the GIJON-2006 experiment we obtained better results when using seasonal coefficients than monthly ones; likewise, the results were improved when using on the continental shelf those coefficients estimated

TABLE 4. – Depth-averaged rms of the difference between measured and estimated Salinity for the six cases considered.

	M	Ss	M-IO	Ss-IO	STM	WOA
GIJON-2006	0.045	0.025	0.027	0.025	0.048	0.050
FINISTERRE-2006	0.063	0.043	–	–	0.070	0.117

with historical data from the interior ocean. *STM* and *WOA05* cases produced in all cases higher average deviations than those obtained for the polynomial cases. The best case in this particular analysis seems to be to estimate the salinity with coefficients obtained with seasonal historical data from the interior ocean in both regions (interior ocean and continental shelf). This means that separating the region of study into the shelf and interior ocean is not necessary or representative of the particular situation of this experiment; a possible explanation for this is the relatively low number of observations available to perform the monthly fits, i.e. the historical database does not reflect the entire variability expected for May. In the spring and summer, with prevailing north-easterly winds in the region, the circulation is roughly westwards along the northern Iberian coast, but it is affected by the intermittent passage of storms (Lavín *et al.*, 2006; Ruiz-Villarreal *et al.*, 2006). This was the case of the GIJON-2006 experiment, which was preceded by the passage of an active atmospheric perturbation from the west associated with a westerly wind pulse of several days that caused either a piling or intrusion of offshore waters over the shelf and constrained fresh water river plumes against the coast (Sotillo *et al.*, 2008). The XBT and CTD sections show waters over the shelf with temperatures relatively colder than the historical data and slightly saltier than usual. The trajectories of the drifters released a day before the hydrographic cruise show surface water parcels moving shoreward from the shelf break (Olivella *et al.*, 2007).

The key variable in the methodology presented here is the salinity, the variable simulated by the polynomial fit and the one we use to validate the methodology. However, a technical unit would expect information on the surface velocity field, a more informative variable in rescue and safety operations. Hence, we present some results on the surface velocity obtained by the CTD salinity data, those estimated with our best polynomial fit (*Ss–IO*) and a third one for the *STM* case. The reference level used for geostrophic calculations is the interface between central and intermediate waters located at nearly 400 m; at stations shallower than this depth, the deepest common depth is used as reference level. Surface geostrophic velocities obtained for the three cases are shown in Figure 11. Note that the estimated fields are rather coherent with respect to geostrophic velocity field derived directly from the complete CTD data. They exhibit the similar spatial structure and, except in some places, the magnitudes are comparable (6-14 cm s^{-1}). Surface velocities recorded by an oceanographic buoy located at Cabo de Peñas (43º73'N, 6º17'W, along the section labelled as I in Fig. 2A) during the CTD survey were about 20 cm s^{-1} on average and peaks of about 35 cm s^{-1} were recorded. In addition, mean velocities from surface drifters deployed during the experiment were about 7-20 cm s^{-1}, which is only slightly larger than geostrophic computations. This suggests that the geostrophic component at the surface was not small but accounted for an important contribution to the total surface velocity.

A propagation of uncertainty analysis is performed to assess how the impact of uncertainty in the salinity determination is translated to the final surface geostrophic velocity field. Salinity values are randomly varied one hundred times within the *a posteriori* error given by the inverse methodology (*STM* case is not considered here), calculating for each case a surface velocity. We obtain a standard deviation in the surface velocity around 0.1 cm s^{-1}. Hence, mean surface values in the best case (*Ss–IO*) are around 10±0.1 cm s^{-1}, very close to values computed from the CTD data with a correlation coefficient (r^2) around 0.81.

FINISTERRE-2006 exercise

During the FINISTERRE-2006 exercise ten XBTs were launched along two nearly-zonal lines, from the continental shelf to the interior ocean (Fig. 2B). The vertical sections of temperature measured by the XBTs are shown in Figure 12. Surface warming is still present during November in the upper 100 m at both sections, reaching 19ºC, a striking feature which is not present in the historical dataset (Fig. 5). At intermediate levels, in the southern section, the increase in temperature with depth seen in the most offshore profile is related to the presence of MW, a feature already described in the historical dataset.

Five XCTDs (model XCTD-2, maximum depth 1850 m) were launched in the region, three in the northern section and two in the southern one, meas-

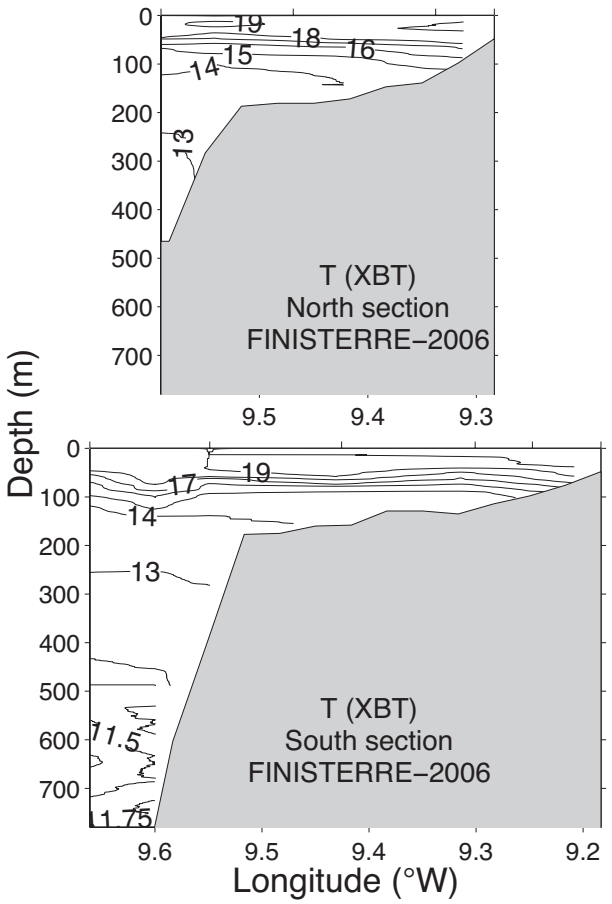

FIG. 12. – Vertical sections of temperature measured by XBTs during the FINISTERRE-2006 field exercise in the northern and southern sections as a function of longitude.

uring temperature and salinity in the upper 1000-1800 m of the interior ocean (Fig. 2B). This limits the validation of the polynomial coefficients to only the interior ocean cases (*M* and *Ss*). Figure 13 shows the XCTD observations on a TS diagram, where we again note the surface warming up to nearly 19ºC and the presence of MW at intermediate levels in both northern and southern sections, with salinity rising to nearly 36.

The results after calculating salinity with polynomial coefficients corresponding to cases *M* and *Ss* are presented in Figure 14A. We again represent the average rms of the difference between the measured and the estimated salinity, jointly with the results for *STM* and *WOA05*. Here the errors in salinity are generally lower than 0.1, being higher than 0.1 at the near-surface (>100 m) and at depth (<700 m). Higher errors are related to *Ss* and *STM* cases at surface (<100 m), while at intermediate levels the higher deviations are related to the *STM* and *WOA*05 cases. Results averaged over the whole water column are compiled in Table 4, where we observe that the *Ss* case gives better results than the *M* one, with deviations in the order of 0.04 and 0.06, respectively. Depth-averaged errors related to *STM* and *WOA*05 amount to 0.07 and 0.12.

The surface geostrophic velocity is shown in Fig. 14B, where results from CTD observations are compared to the v_g obtained by calculating the sa-

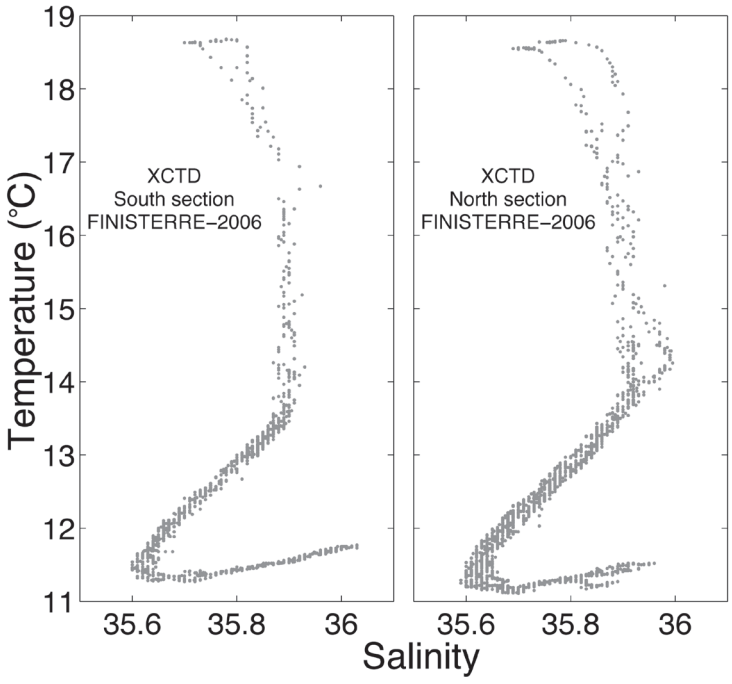

FIG. 13. – TS diagram corresponding to XCTD observations in the southern (left) and northern (right) sections during the FINISTERRE-2006 exercise.

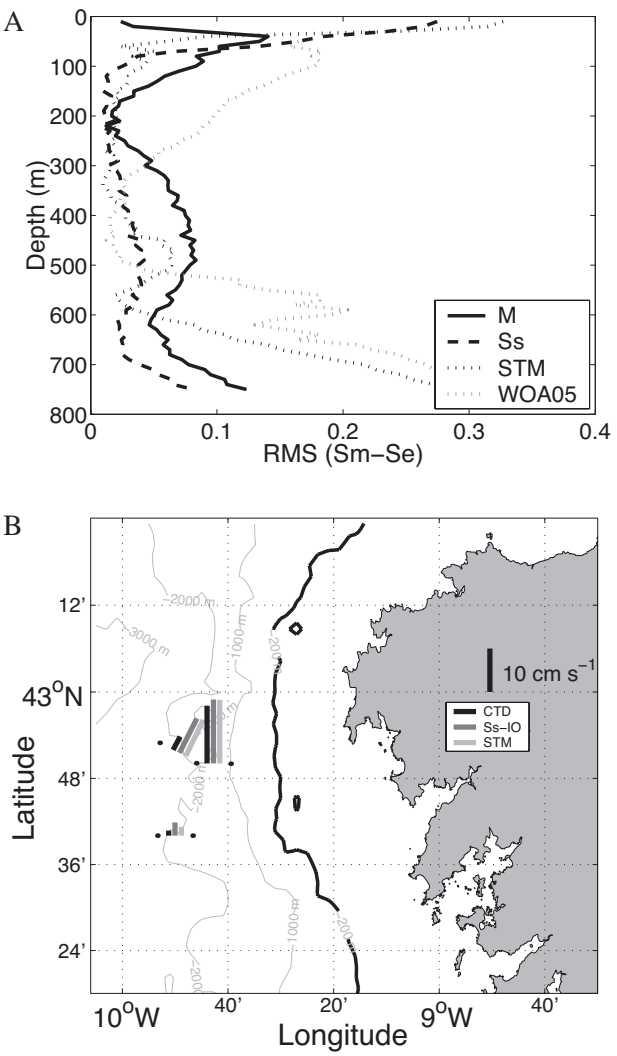

FIG. 14. – A, rms of the difference between measured and estimated salinity (see text for details); B, surface geostrophic velocity during the FINISTERRE-2006 exercise estimated with CTD data and with our best polynomial coefficients (*Ss–IO*).

linity with the *Ss* case. Here the comparison is only restricted to three pairs of stations, with results being similar in one place and overestimated for the rest. Surface velocities are between 1.2 and 13.4 cm s^{-1}, with errors around ±0.1 cm s^{-1} (r^2=0.81). These values are not negligible compared with surface mean velocities obtained from surface drifters released a day before the cruise (around 7.5-20 cm s^{-1}).

DISCUSSION

From an operational point of view, the results for recovering salinity through the adjustment of a polynomial fit to historical T-S relationships are quite straightforward. A set of coefficients has been computed and proposed for practical use distinguishing two seasons (summer-like and winter-like), two different regions (the Galician Area and the Cantabrian Sea) and two dynamically different areas (the continental shelf and the interior ocean). The validation of the methodology in both exercises showed that better results were obtained using seasonal coefficients rather than monthly coefficients, perhaps due to the lack of representativeness of monthly datasets compared to seasonal datasets. Using a seasonal dataset separation, errors in recovering the salinity at the surface were greater than at intermediate levels (roughly between 100 and 600 m), being lower than 0.05 in both exercises. In the GIJON-2006 exercise, the best fit was achieved when the coefficients from the interior ocean region were also used for recovering the salinity over the shelf area. This does not mean that the separation is useless but that, due to the particular dynamics during the experiment (after a wind storm), offshore waters seemed to have intruded over the shelf, a circumstance that may explain the offshore character of the shelf thermohaline properties. At deeper levels, errors tend to be greater due to the detected intrusion of Mediterranean Water that appears to be undersampled in the historical dataset.

Concerning the surface geostrophic velocities, in both exercises a relatively high correlation and general agreement are obtained between velocity values computed from the CTD and XCTD observations and those calculated using measured temperature profiles with salinity profiles estimated through the polynomial fit. According to the results, for the exercises here analysed such values are non-negligible with respect to the velocities from other direct and indirect observations (an oceanographic buoy and surface drifters), indicating that the geostrophic component at the surface may make an important contribution to the total surface velocity; this should be carefully taken into account when dispersion models are used at the surface. In summary, with enough historical data the salinity field can be recovered reasonably well and a rather simple methodology like the one presented here performs well in providing first diagnostics of the velocity in the upper levels.

Improvements can be made in several ways: for example, by implementing more sophisticated methods such as EOF decomposition (Maes *et al.*, 2000) and neural networks (Krasnopolsky *et al.*, 2000), or using more general regression models with complementary variables (Thacker and Sindlinger, 2007, i.e.

latitude, sea surface salinity, etc.). Further research can be made in these directions to determine whether the improvements achieved by more complex methods compensate for the additional needs of greater datasets or the use of additional variables such as sea surface height or sea surface salinity.

Now that salinity is to be synoptically recovered through the SMOS (Font *et al.*, 2004) and AQUARIUS satellite missions (Koblinsky *et al.*, 2003), the problem of finding the sea surface density and therefore the sea surface velocity should be solved. However, the expected coarse resolutions and accuracy will prevent its use for operational purposes such as marine emergencies. As an alternative, a compensated velocity field may also be obtained through techniques of data assimilation into a forecast system running operationally in the area of an emergency. In this case it would be desirable to analyse the impact of just assimilating real-time XBT data. Unfortunately this was not possible in the exercises presented here and is therefore left for future work.

Based on these results and the experience acquired during these two exercises, we recommend to a technical unit that a rapid sampling using XBT probes can produce very useful results given the expected constraints in marine emergencies. XCTDs can be easily integrated into marine emergency exercises and are a key element for validating the salinity recovery performed by the inverse methodology, increasing the reliability of the whole process. The resources needed with the adapted autonomous system are not demanding and XBT sampling can be used in an opportunistic way (normal rescue boats), without significantly impacting the operations usually carried out during marine emergencies. The methodology presented here can therefore be easily extended to other regions characterised by dense ship traffic with a high risk of accidents or under rough weather conditions. As an example, the XBT sampling in the GIJON-2006 experiment was done under a strong groundswell after an atmospheric perturbation that prevented a normal CTD cruise from being carried out.

ACKNOWLEDGMENTS

We would like to thank the ESEOO Project (VEM2003-20577-C14) for providing the framework in which this study was carried out. Many thanks are also due to SASEMAR for making available the logistic in the field exercises and to Hydrobase for making available the historical data. We also thank the crew of the R/V José de Rioja and the IEO (Instituto Español de Oceanografía) for participating in the GIJON-2006 experiment and providing the CTD data used in this study. We appreciate the comments made by two anonymous reviewers who helped to improve the final version of the manuscript. The first author would like to thank the CANOA Project (CTM2005-00444/MAR) and Juan de la Cierva Programme, both funded by the Spanish Ministry of Education and Science, for supporting him while working on this study.

REFERENCES

Álvarez, E., I. Losada, J. Tintoré, J. Menéndez, M. Espino, G. Parrilla, I. Martínez and V. Pérez-Muñuzuri. – 2007. *The ESEOO Project: developments and perspectives for Operational Oceanography at Spain*. Proceedings of ISOPE-2007: The 17th International Offshore Ocean and Polar Engineering Conference, Lisbon, Portugal.

Antonov, J.I., R.A. Locarnini, T.P. Boyer, A.V. Mishonov and H.E. Garcia. – 2006. World Ocean Atlas 2005, Volume 2: Salinity. Technical Report 62, NOAA Atlas NESDIS 62, Washington D.C.

Caballero, A., M. Espino, Y. Sagarminaga, L. Ferrer, A. Uriarte and M. González. – 2008. Simulating the migration of drifters deployed in the Bay of Biscay, during the Prestige crisis. *Mar. Pollut. Bull.*, 56(3): 475-482.

Carracedo, P., S. Torres-López, M. Barreiro, P. Montero, C. Balseiro, E. Penabad, P. Leitao and V. Pérez-Muñuzuri. – 2006. Improvement of pollutant drift forecast system applied to the Prestige oil spills in Galicia Coast (NW of Spain): Development of an operational system. *Mar. Pollut. Bull.*, 53: 350-360.

Castanedo, S., R. Medina, I. Losada, C. Vidal, F. Méndez, A. Osorio, J. Juanes and A. Puente. – 2006. The Prestige oil spill in Cantabria (Bay of Biscay). Part I: Operational forecasting system for quick response, risk assessment, and protection of natural resources. *J. Coast. Res.*, 22(6): 1474–1490.

Daniel, P., P. Josse, P. Dandin, J. Lefevre, G. Lery, F. Cabioch and V. Gouriou. – 2004. *Forecasting the Prestige oil spill*, Interspill 2004 Conference, Trondheim, Norway. http://www.meteorologie.eu.org/mothy/references/Interspill_2004.pdf

Emery, W.J. – 1975. Dynamic height from temperature profiles. *J. Phys. Oceanogr.*, 5: 369-375.

Emery, W.J. and J.S. Dewar. – 1982. Mean temperature-salinity, salinity-depth and temperature-depth curves for the North-Atlantic and the North Pacific. *Prog. Oceanogr.*, 11: 219-305.

Fiúza, A. and D. Halpern. – 1982. Hydrographic Observations of the Canary Current Between 21ºN and 25.5ºN in March/April 1974. *Rapp. p-v. Réun.*, 180: 58–64.

Flierl, G.R. – 1978. Correcting expandable bathythermograph (XBT) data for salinity effects to compute dynamic heights in Gulf Stream rings. *Deep-Sea Res. Part. I*, 25: 129-134.

Font, J., G. Lagerloef, D. Le Vine, A. Camps and O.-Z. Zanifé. – 2004. The determination of surface salinity with the European SMOS Space Mission. *IEEE Trans. Geosci. Remote*, 42(10): 2196-2205.

González-Pola, C., A. Lavín and M. Vargas-Yáñez. – 2005. Intense warming and salinity modification of intermediate water masses in the southeastern corner of the Bay of Biscay for the period 1992-2003. *J. Geophys. Res. C*, 110(C05020), 10.1029/2004JC002367.

Hackett, B. – 2004. The impact of global ocean model forcing data on oil spill fate prediction: a comparative study of the 'Prestige' accident. Technical Report 13, Norwegean Meteorological Institute.

http://met.no/english/r_and_d_activities/publications/2004/13_2004/013-2004.pdf
Hansen, D.V. and W.C. Thacker. – 1999. Estimation of salinity profiles in the upper ocean. *J. Geophys. Res. C*, 104(C4): 7921-7933.
Harvey, J. – 1982. θ-S relationships and water masses in the eastern North Atlantic. *Deep-Sea Res. Part A*, 29(8A): 1021-1033.
Kessler, W. and B. Taft. – 1987. Dynamic heights and zonal geostrophic transports in the central Pacific during 1979–84. *J. Phys. Oceanogr.*, 17: 97-122.
Koblinsky, C., P. Hildebrand, D. Le Vine, F. Pellerano, Y. Chao, W. Wilson, S. Yueh and G. Lagerloef. – 2003. Sea surface salinity from space: Science goals and measurement approach. *Radio Sci.*, 38, doi:10.1029/2001RS002584: 8064.
Krasnopolsky, V., D. Chalikov, L. Breaker and D. Rao. – 2000. *Application of neural networks for efficient calculation of sea water density or salinity from the UNESCO equation of state*. Long Beach, CA (USA), pp. 27-30.
Lagerloef, G., C. Swift and D. LeVine. – 1995. Sea Surface Salinity: the next remote sensing challenge. *Oceanography*, 8: 44-50.
Lavín, A., L. Valdés, F. Sánchez, P. Abaunza, A. Forest, J. Boucher, P. Lazure and A. Jegou. – 2006. *The Sea Volume 14B: The Global Coastal Ocean. Interdisciplinary Regional Studies and Syntheses*, chapter The Bay of Biscay: the encountering of the ocean and the shelf. Harvard University Press.
Locarnini, R.A., A.V. Mishonov, J.I. Antonov, T.P. Boyer and H. E. Garcia. – 2006. World ocean atlas 2005, volume 1: Temperature. Technical report, NOAA Atlas NESDIS 61, Washington D.C.
Maes, C., D. Berhinger, R. Reynolds and M. Ji. – 2000. Retrospective analysis of the salinity variability in the Western tropical Pacific Ocean using an indirect minimization approach. *J. Atmos. Oceanic Technol.*, 17: 512–5243.
Marrero-Díaz, A. – 2002. *Acoplamiento entre el giro subtropical del Atlántico Norte y el afloramiento costero en el noroeste africano*. Ph.D. thesis, Univ. Las Palmas de Gran Canaria.
Marrero-Díaz, A., J.L. Pelegrí, A. Rodríguez-Santana and P. Sangrà. – 2001. Applicability of T-S algorithms to the Canary Islands region. *Sci. Mar.*, 65(S1): 195–204.
Marrero-Díaz, A., A. Rodríguez-Santana, F. Machín and J.L. Pelegrí. – 2006. Analitic salinity-temperature relations for the upper thermocline waters of the eastern North Atlantic subtropical gyre. *Sci. Mar.*, 70(2): 167-175.
Menke, W. – 1984. *Geophysical Data Analysis: Discrete Inverse Theory*. Academic Press, INC., Orlando, 46.
Montero, P., J. Blanco, J. Cabanas, J. Maneiro, Y. Pazos, A. Moroño, C. Balseiro, P. Carracedo, B. Gomez, V. Penabad, V. Perez-Muñuzuri, F. Braumschweig, R. Fernandes, P. Leitao and R. Neves. – 2003. *Oil Spill Monitoring and Forecasting on the Prestige-Nassau Accident*, volume 2, 26th Arctic and Marine Oil Spill Program (AMOP). http://www.meteogalicia.es/galego/informacion/documentos/AMOP.pdf
Olivella, R., E. García-Ladona, J. Salat, A. Julià and E. del Río. – 2007. Lagrangian buoys tracking system: Operational exercises. Technical report, ESEOO Technical Report. http://www.icm.csic.es/oce/people/emilio/papers/Olivella-etal-2006-IT.pdf
Pérez, F.F., A. Ríos, B. King and R. Pollard. – 1995. Decadal changes of the θ-S relationship of the eastern North Atlantic Central Water. *Deep-Sea Res. Part I*, 42(11/12): 1849-1864.
Ríos, A.F., F.F. Pérez and F. Fraga. – 1992. Water masses in the upper and middle North Atlantic Ocean east of the Azores. *Deep-Sea Res. Part I*, 39: 645-658.
Ruiz-Villarreal, M., C. González-Pola, G. Díaz del Río, A. Lavín, P. Otero, S. Piedracoba and J. Cabanas. – 2006. Oceanographic conditions in North and Northwest Iberia and their influence on the Prestige oil spill. *Mar. Pollut. Bull.*, 53: 220-238.
Sabia, R., A. Camps, M. Vall-Ilossera and N. Reul. – 2006. Impact on sea surface salinity retrieval of different auxiliary data within the SMOS mission. *IEEE Trans. Geosci. Remote*, 44(10): 2769–2778.
Siedler, G. and L. Stramma. – 1983. The applicability of the T/S method to geopotential anomaly computations in the northeast Atlantic. *Oceanol. Acta*, 6(2): 167-172.
Sotillo, M.G., E. Álvarez, S. Castanedo, A. Abascal, J. Menéndez, M. Emelianov, R. Olivella, E. García-Ladona, M. Ruiz-Villareal, J. Conde, M. Gómez, P. Conde, A. Gutierrez and R. Medina. – 2008. Towards an operational system for oil spill forecast over Spanish waters: initial developments and implementation test. *Mar. Pollut. Bull.*, 56.
Stommel, H. – 1947. Note on the use of T/S correlation for dynamic height anomaly computations. *J. Mar. Res.*, 6(2): 85-92.
Thacker, W. and L. Sindlinger. – 2007. Estimating salinity to complement observed temperature: 2. Northwestern Atlantic. *J. Mar. Sys.*, 65: 249-267.
Thacker, W.C. – 2007. Estimating salinity to complement observed temperature: 1. Gulf of Mexico. *J. Mar. Sys.*, 65: 224-248.
van Aken, H. – 2000. The hydrography of the mid-latitude northeast Atlantic Ocean II: The intermediate water masses. *Deep-Sea Res. Part I*, 47: 789–824.
van Aken, H. 2001. The hydrography of the mid-latitude Northeast Atlantic Ocean – Part III: the subducted thermocline water mass. *Deep-Sea Res. Part I*, 48: 237-267.
van Aken, H. – 2002. Surface currents in the Bay of Biscay as observed with drifters between 1995 and 1999. *Deep-Sea Res. Part I*, 49(6): 1071-1086.
Wilkin, J., H. Arango, D. Haidvogel, C. Lichtenwalner, S. Glenn and K. Hedstrom. – 2005. A regional ocean modeling system for the Long-term Ecosystem Observatory. *J. Geophys. Res. C*, 110(C6): C06S91.

Scient. ed.: J. Font.
Received June 26, 2007. Accepted June 25, 2008.
Published online October 24, 2008.